

## THE MYSTERY OF THE $\sigma$ -BUMP – A NEW SIGNATURE FOR MAJOR MERGERS IN EARLY-TYPE GALAXIES?

ANNA THERESE PHOEBE SCHAUER<sup>1</sup>, RHEA-SILVIA REMUS<sup>1,2</sup>, ANDREAS BURKERT<sup>1,2</sup> AND PETER H. JOHANSSON<sup>3</sup>

<sup>1</sup> Universitäts-Sternwarte München, Scheinerstr. 1, D-81679 München, Germany

<sup>2</sup> Max-Planck-Institute for Extraterrestrial Physics, P.O. Box 1312, D-85748 Garching, Germany

<sup>3</sup> Department of Physics, University of Helsinki, Gustaf Hällströmin katu 2a, FI-00014 Helsinki, Finland  
aschauer@usm.uni-muenchen.de

*Draft version June 25, 2021*

### ABSTRACT

The stellar velocity dispersion as a function of the galactocentric radius of an early-type galaxy can generally be well approximated by a power law  $\sigma \propto r^\beta$ . However, some observed dispersion profiles show a deviation from this fit at intermediate radii, usually between one and three  $R_{\text{eff}}$ , where the velocity dispersion remains constant with radius, showing a bump-like behavior, which we term the “ $\sigma$ -bump”. To understand the origin of this  $\sigma$ -bump, we study a set of simulated early-type galaxies formed in major mergers. We find the  $\sigma$ -bump in all of our simulated early-type galaxies, with the size and position of the bump slightly varying from galaxy to galaxy, leading to the assumption that the bump is a characteristic of the major merger formation scenario. The feature can be seen both in the intrinsic and projected stellar velocity dispersions. In contrast to shells that form during the merger event but evolve with time and finally disappear, the  $\sigma$ -bump stays nearly constant with radius and is a permanent feature that is preserved until the end of the simulation. The  $\sigma$ -bump is not seen in the dark matter and gas components and we therefore conclude that it is a purely stellar feature of merger remnants.

*Subject headings:* galaxies: kinematics and dynamics — galaxies: elliptical and lenticular, cD — methods: numerical

### 1. INTRODUCTION

The kinematics of early-type galaxies (ETGs) has been a subject of interest for many years. Unfortunately, the stellar light decreases rapidly after one to two effective radii, allowing observations to reliably detect only the inner effective radii (Proctor et al. 2009; Foster et al. 2013; Arnold et al. 2013). Thus, the outer halos cannot be studied by observing the stellar light directly.

However, there are several reasons why the outer regions are of interest, especially as this is where the dark matter becomes dominant and its properties can be tested. Romanowsky et al. (2003) for example found a steep Keplerian decline in the velocity dispersion of NGC 3379, resulting in discussions about the existence of a canonical dark halo (Dekel et al. 2005; Douglas et al. 2007). In addition, the kinematics of the stellar component in the regions far away from the center are most likely to preserve some indications of the formation history of the galaxy. For example, in S0-galaxies, the distinction between random motion and the ordered motion of a kinematically cold stellar disk component can reveal if the galaxy is actually a fading spiral galaxy or was formed from a minor merger, as discussed by Noordermeer et al. (2008); Cortesi et al. (2013).

In order to study ETGs to larger radii, tracers are needed. These tracers need to emit enough light to be detectable as single objects even at large distances. Currently the most important tracers are planetary nebulae (PNe) and globular clusters (GCs). Planetary nebulae emit a large amount of their light in the [O III] $\lambda$ 5007 line and can therefore be observed out to many effective radii, as seen in the famous example of NGC 5128 where plane-

tary nebulae have been found out to 20 kpc by Hui et al. (1995) and out to 80 kpc by Peng et al. (2004). With spectrographs it is now possible to obtain not only the positions but also the line-of-sight velocities of hundreds of objects far away from the center (e.g. Méndez et al. (2009): 591 PNe in NGC 4697, Coccato et al. (2009): 450 PNe in NGC 4374).

Another possible tracer for the stellar dynamics in the outskirts of ETGs is GCs. Two groups of GCs can be distinguished: red, metal-rich GCs and blue, metal-poor GCs. Studies by Schuberth et al. (2010) and others provide evidence that the stellar field population is traced by red GCs, whereas blue globular clusters may have been accreted later. A total of more than 2500 GCs have been studied recently by Pota et al. (2013) in 12 nearby ETGs.

In numerical simulations, one is not restricted by the decreasing surface brightness, but by resolution effects. However, with improved numerical techniques, the analysis of small scale details of ETGs is now possible. For example, the shell-structure of ETGs, first observed in NGC 1316 by Malin (1977), could be understood to be due to disruption of an accreted galaxy by mergers (e.g. Toomre 1978; Schweizer 1986; Hernquist & Quinn 1988; Binney & Tremaine 2008; Cooper et al. 2011) into the host galaxy. Therefore, these shell-structures can reveal information about the merger history of the galaxy.

To have a further indicator for the formation history of ETGs, we study in this Letter the velocity dispersions of merger remnants. The goal is to find residual kinematic signatures of the progenitor galaxies that are still detectable despite the violent relaxation experienced by

the merging galaxies.

## 2. SIMULATIONS

We study ten ETGs formed in isolated major mergers of both spiral-spiral and spiral-elliptical galaxies. For the simulations, we used the parallel TreeSPH-code Gadget-2 (Springel 2005), in which energy and entropy are manifestly conserved, including radiative cooling of a primordial hydrogen-helium composition. Star formation and supernova feedback were included, using the self-regulated model of Springel & Hernquist (2003). The description of the interstellar medium is based on a two-component model, where cool clouds are embedded in a surrounding medium of hot gas (McKee & Ostriker 1977; Johansson & Efstathiou 2006).

Nine out of our ten galaxies include a black hole. For modelling its feedback, we used the model of Springel et al. (2005). To guarantee efficient merging in the simulations, BHs merge instantaneously as soon as one BH is within the other BH's smoothing length and its velocity has become smaller than the local sound speed of the surrounding particles. The progenitor disk galaxies are embedded in Hernquist like dark matter halos with concentration parameters  $c_s = 9$  of the corresponding NFW-halo (Navarro et al. 1997). The baryonic disk scale-radius is  $r_D = 3.5$  kpc. For more details on the simulations, see Johansson et al. (2009a), Johansson et al. (2009b) and Remus et al. (2013).

Our sample consists of 5 spiral-spiral mergers with a mass ratio of 1:1 for the progenitors and 4 mergers with a ratio of 3:1, as well as one mixed merger (spiral and elliptical formed by a 3:1 spiral-spiral merger). The merger parameters are described in detail in Table 1. To demonstrate our analysis, we use the 1:1 spiral-spiral merger 11 OBH 13 as an example galaxy, which has the following initial setup: inclinations  $i_1 = -109^\circ$  and  $i_2 = 180^\circ$ , pericenter arguments  $\omega_1 = 60^\circ$  and  $\omega_2 = 0^\circ$ ,  $v_{vir} = 160 \text{ km s}^{-1}$ .

## 3. RESULTS

Observations have shown that the projected velocity dispersion (= root mean squared velocity) of the stellar component can in general be well-fitted by a power-law (Douglas et al. 2007; Napolitano et al. 2009)

$$\sigma \propto r^\beta, \quad (1)$$

We calculate the intrinsic velocity dispersion profiles for our spheroidals and fit a power-law to the stellar component. Therefore, each directional component of the velocity dispersion is computed in radial bins as

$$\sigma_i(r) = \sqrt{\frac{\sum v_i(r)^2}{N} - \left(\frac{\sum v_i(r)}{N}\right)^2}, \quad (2)$$

where the sum runs over all particles within the bin. The intrinsic velocity dispersion is then calculated as

$$\sigma = \sqrt{\sigma_1^2 + \sigma_2^2 + \sigma_3^2}. \quad (3)$$

The upper panel of Figure 1 shows the velocity dispersion of the stellar and dark matter component of

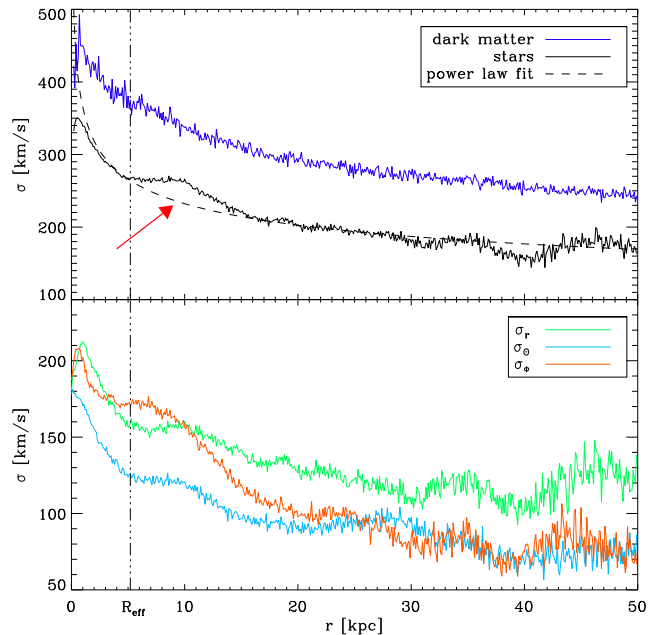


FIG. 1.— Upper panel: Stellar (black) and dark matter (blue) intrinsic velocity dispersion as function of radius for galaxy 11 OBH 13. For the stellar component, the power law fit is included (black dashed curve). The  $\sigma$ -bump (red arrow) as a positive deviation from a power-law behavior only shows in the stellar component. Lower panel: Radial (green), tangential (blue) and azimuthal (orange) components of the stellar velocity dispersion.

our example galaxy, 11 OBH 13, as a function of radius, together with a power-law fit to the stellar component. For our sample of spheroidals, we find the mean of the power law exponent to be  $\beta = -0.18 \pm 0.04$  for the stellar component (see Table 1). This is in agreement with the stellar slope of Dekel et al. (2005) ( $\beta = -0.4 \pm 0.1$  in projection) and slightly below the values found in hydrodynamical cosmological zoom-in simulations ( $\beta = -0.05 \pm 0.06$ ) and large-scale hydrodynamical cosmological simulations ( $\beta = -0.003 \pm 0.135$ ) of Remus et al. (2013).

We include more than 680 000 (450 000) stellar particles in each 1:1 (3:1) ETG, with each bin having a bin-width of 0.1 kpc and containing more than 1000 particles for radii up to 20 kpc. To ensure that our results do not depend on the binning, we tested equal-mass bins (1500 particles per bin) and other equal-radius binwidths, but found no differences.

As can be seen in Figure 1, the stellar velocity dispersion generally follows the power law, but shows some deviations. The innermost deviation of the velocity dispersion from a power-law within 2 kpc is due to very bound bulge-stars in the deep gravitational potential at the galaxies' center. Here, we are not interested in the bulge component and therefore neglect the innermost radii. Other deviations from the power-law are caused by shell-structures. Shells can form in major mergers, e.g. described by Cooper et al. (2011), leading to an ejection of stars in density waves (Schweizer 1986). Therefore, the velocity dispersion varies at the radii where shells are present.

We distinguish between the deviation in the range of 5 to 15 kpc and the oscillations at larger radii. The latter

TABLE 1  
BINARY MERGER SIMULATION SAMPLE AT A TIMESTEP OF 3 GYR

Model	Ratio <sup>(a)</sup>	Orbit <sup>(b)</sup>	$f_{\text{gas}}$ <sup>(c)</sup>	bulge <sup>(d)</sup>	BH <sup>(e)</sup>	$v_{\text{vir}}$ <sup>(f)</sup>	$R_{\text{eff}}$ <sup>(g)</sup>	$\beta$ <sup>(h)</sup>
11 NB NG 13	1:1	G13	0.0	no	yes	160	8.48	-0.17
11 NB OBH 13	1:1	G13	0.2	no	yes	160	6.15	-0.19
11 NG 13	1:1	G13	0.0	yes	yes	160	6.76	-0.17
11 OBH 09	1:1	G09	0.2	yes	yes	160	5.02	-0.22
11 OBH 13	1:1	G13	0.2	yes	yes	160	5.20	-0.20
31 ASF 01	3:1	G01	0.2	yes	no	160	4.59	-0.21
31 O8BH 13	3:1	G13	0.8	yes	yes	160	2.56	-0.19
31 OBH 09 320	3:1	G09	0.2	yes	yes	320	10.42	-0.10
31 OBH 13	3:1	G13	0.2	yes	yes	160	5.22	-0.18
mix 11 OBH 13	1:1	G13	0.2	yes	yes	160	6.32	-0.18

NOTE. — (a) initial mass ratio of the two galaxies; (b) Orbit type according to Naab & Burkert (2003); Naab et al. (2006); Khochfar & Burkert (2006); (c) Initial gas fraction of the disks of the progenitor galaxies; (d) Do the progenitor galaxies contain a Bulge? (e) Do the progenitor galaxies contain Black Holes? (f) Initial virial velocity in  $\text{km s}^{-1}$ ; (g) Effective Radius in kpc at 3 Gyrs; (h) Slope for fitting  $\sigma \propto r^\beta$  to the stellar component of the velocity dispersion at 3 Gyrs in the range of 0–50 kpc;

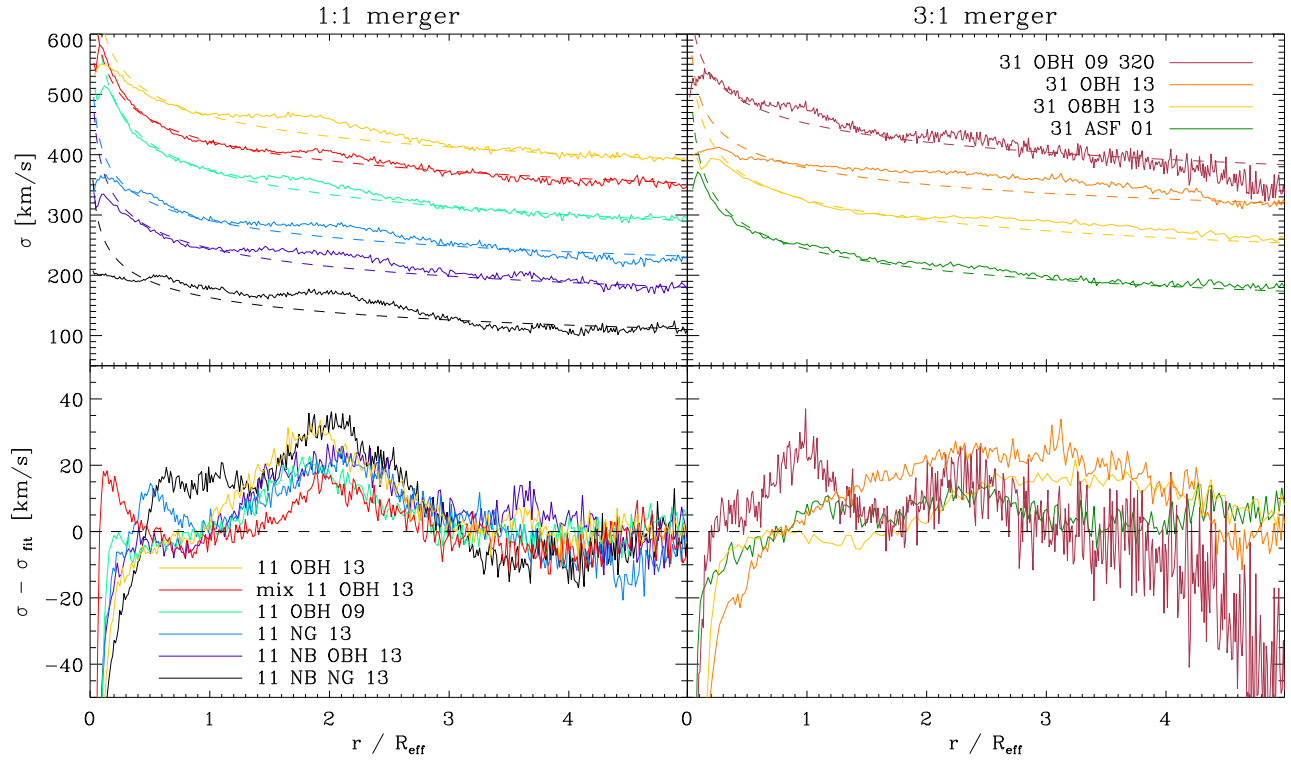


FIG. 2.— Left column: 1:1 mergers, right column: 3:1 mergers (all at 3 Gyrs). Upper panels: Velocity dispersion of the different spheroids (solid lines) and their corresponding power laws (dashed lines) as function of effective radius. For better readability, we shift the dispersion profiles for all mergers except 11 NB OBH 13, 31 ASF 01 and 31 O8BH 09 320 by factors of 50. The lower panel displays the difference between the velocity dispersion and its best fit power-law.

are clearly linked to regions of high particle density, visually identified as shell-structures. In the region between 5 and 15 kpc, where  $\sigma$  stays constant up to 11 kpc and then decreases rapidly to follow the power law again, no shell feature can be identified in the simulations. Therefore, the deviation must have another origin and we call it  $\sigma$ -bump.

In the dark matter component, the velocity dispersion is much higher, following a power law without significant deviations, showing no signature of the  $\sigma$ -bump (see upper panel of Figure 1). The stellar components of our other nine galaxies also show a  $\sigma$ -bump (see Figure 2), including some simulations without gas or without a bulge.

The mergers with mass ratio of 1:1 show a more prominent  $\sigma$ -bump than the mergers with mass ratio of 3:1. We therefore conclude that the  $\sigma$ -bump is a purely stellar feature common in our major merger sample and is dependent on the mass ratio of the progenitor galaxies.

The lower panel of Figure 1 shows the radial, tangential and azimuthal component of the velocity dispersion of our example galaxy against radius. The  $\sigma$ -bump is most prominent in the azimuthal component, whereas for larger radii, the deviations from the power law are dominated by the radial component and therefore can be associated with the drift of the shell-structures. A feature like the  $\sigma$ -bump, which is most prominent in the az-

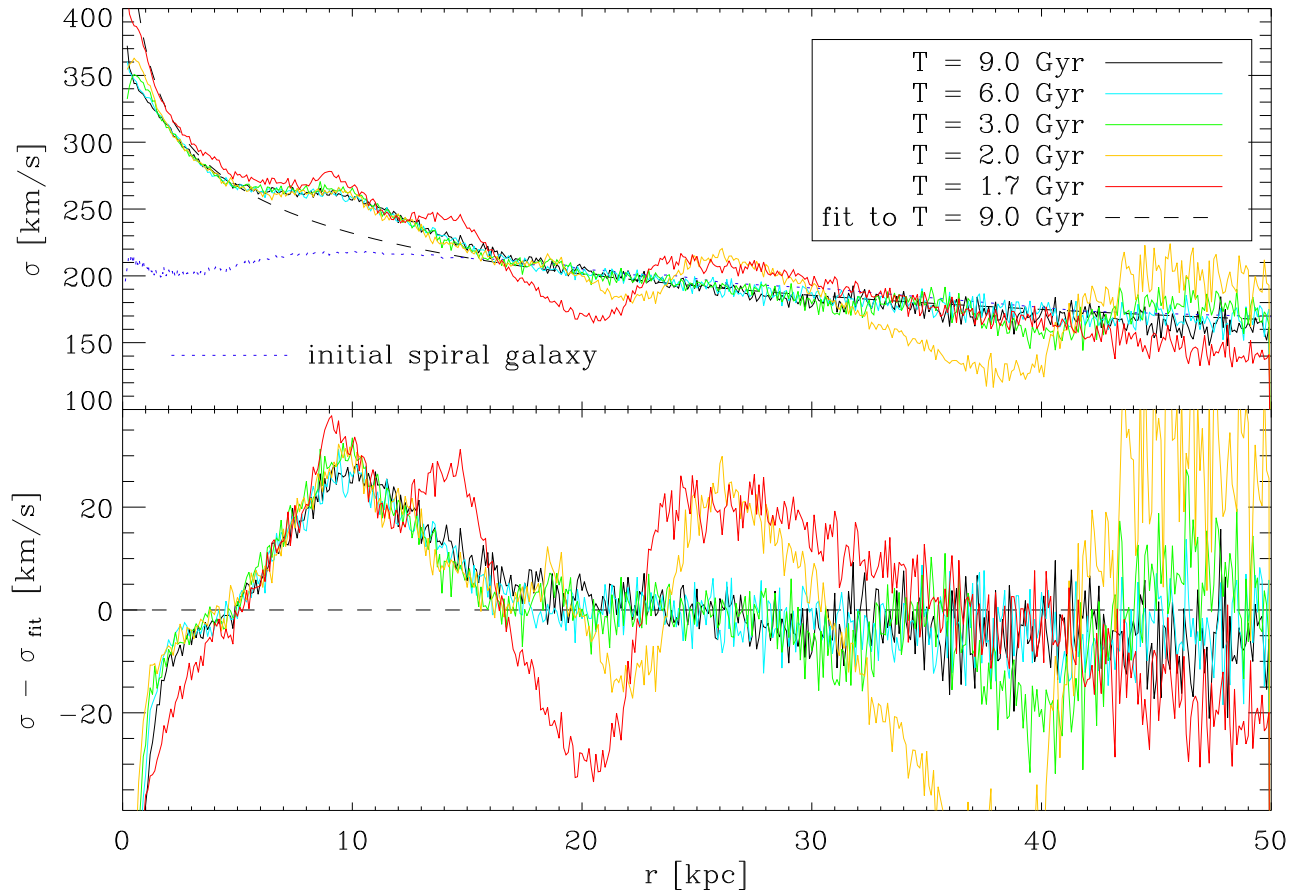


FIG. 3.— Upper panel: Intrinsic stellar velocity dispersion of the example galaxy against radius, different colors indicate different time steps of the simulation (merger encounter at 1.5 Gyrs), intrinsic stellar velocity dispersion of the progenitor spiral galaxy (blue dashed line). Lower panel: Difference of the intrinsic stellar velocity dispersion to the power-law fit of the last snapshot for different time steps (colors same as upper panel).

inmuthal component, could be caused by a disk-structure embedded in the ETG.

In order to understand the origin of the  $\sigma$ -bump and to analyse its shape and size, we investigate the velocity dispersion at different timesteps. The majority of our simulations run for 3.0 Gyrs, with the merger taking place at about 1.5 Gyrs for all galaxies, simulation 11 OBH 13 is run for 9.0 Gyrs.

The upper panel of Figure 3 shows the stellar velocity dispersion of galaxy 11 OBH 13 at different times, indicated by different colors, from 1.7 Gyrs (red curve) to 9.0 Gyrs (black curve). The velocity dispersion of the progenitor spiral galaxy is included as blue dotted line. The  $\sigma$ -bump is not present in the progenitor disks, it is a feature of the merger remnant alone. At the first shown timestep, it is still forming, but from 2.0 Gyrs onwards, the  $\sigma$ -bump remains constant at all times, and thus differs clearly from all the other deviations present at larger radii, which vary or propagate outwards and disappear after some time. This is emphasized in the lower panel of Figure 3, where the difference of the stellar velocity dispersion with respect to the power law fit of the final timestep is shown. Here, we can see more clearly that the  $\sigma$ -bump remains the same in size and shape, while the shell-structures vanish with time.

#### 4. COMPARISON TO OBSERVATIONS

To compare our results to observations it is not sufficient to just consider the intrinsic stellar velocity dispersion, but also its projections. Figure 4 shows the line-of-sight velocity dispersion for different projections from face-on ( $0^\circ$ ) to edge-on ( $90^\circ$ ) in different colors against radius for our example galaxy, as well as the intrinsic velocity dispersion and its power-law fit. The  $\sigma$ -bump can be seen in all line-of-sight velocity projections, although with a somewhat lower amplitude and should therefore be detectable by observations.

We compare our simulations with results from radial velocity measurements of PNe and red GCs in ETGs, as the red GCs are presumed to trace the stellar component of ETGs. We use the position and velocity measurements of the observers to calculate the velocity dispersion as a function of radial distance. For most of the observed galaxies currently available, the observational data sets are not sufficient: either the total sample of tracers contains less than 200 objects, or the data mainly trace radii at which we do not expect to see the  $\sigma$ -bump.

Pota et al. (2013) recently published the kinematics of a sample of globular clusters in 12 ETGs from a spectroscopic survey (see also Strader et al. 2011; Arnold et al. 2011; Foster et al. 2011). The sample of PNe data from



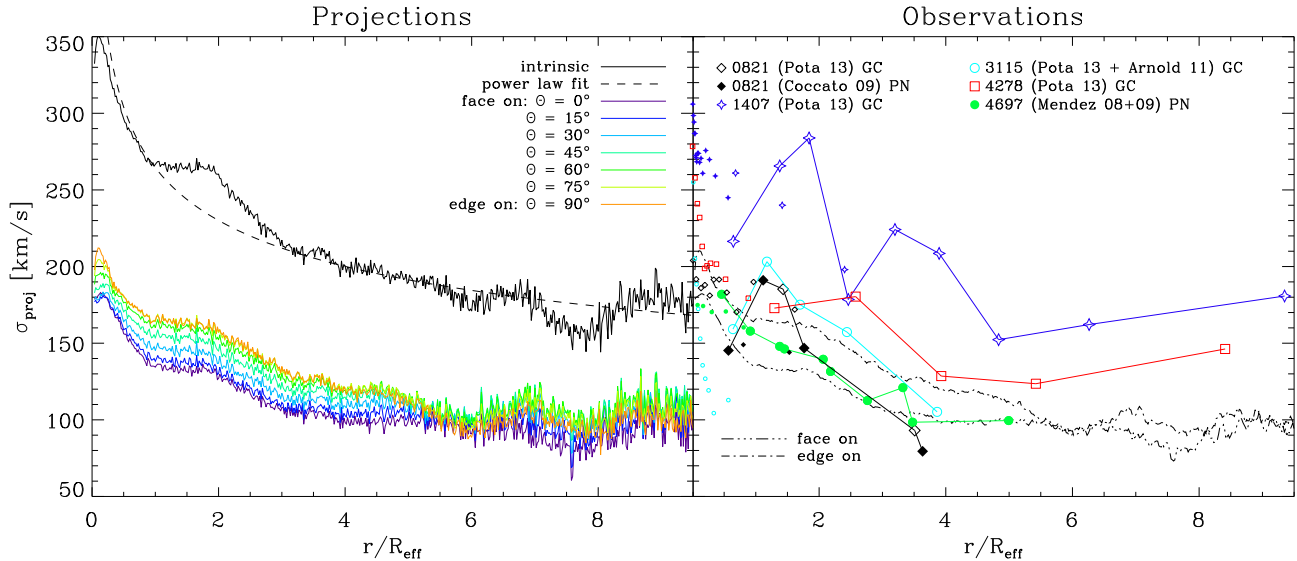


FIG. 4.— Left panel: Stellar velocity dispersion against radius of example galaxy 11 OBH 13. Black line: intrinsic stellar component, black dashed line: power law fit to intrinsic stellar component, dark violet: face on projection, orange: edge on projection, other colors: projections at different angles. Right panel: GCs and PNe are shown by large symbols, additional stellar data by small symbols of the same kind and color (stellar data for NGC 821 from Forestell & Gebhardt (2010) (open diamonds) and Proctor et al. (2009) (filled diamonds), for NGC 1407 from Proctor et al. (2009) (open stars) and Spolaor et al. (2008) (filled stars), for NGC 3115 from Norris et al. (2006), for NGC 4278 from van der Marel & Franx (1993), for NGC 4697 from Binney et al. (1990)). We include the face-on and edge-on projections of the simulated example galaxy as dash-dotted lines.

Coccato et al. (2009) is of similar size, however here we focus on the sample of Pota et al. (2013). We find a  $\sigma$ -bump in four of the twelve galaxies (NGC 821, NGC 1407, NGC 3115, NGC 4278) from this sample, while three other galaxies do not show a significant comparable feature but a constant or decreasing velocity dispersion. For the remaining five galaxies we cannot draw any firm conclusion as we are limited by low-number statistics (37 and 42 red GCs in NGCs 1400 and 2768, respectively, and 21 GCs in NGC 7457), the feature varies a lot with binsize (NGC 4486) or is observed at too large radii (NGC 5846). We include in Figure 4 the observed galaxies which show a  $\sigma$ -bump at the location of the  $\sigma$ -bump of our simulated galaxy 11 OBH 13:

For NGC 821, both PNe and red GCs trace a  $\sigma$ -bump behavior between 0.5 and 1.8  $R_{\text{eff}}$  ( $R_{\text{eff}} = 5.79$  kpc, PNe data from Coccato et al. 2009, GCs data from Pota et al. 2013, stellar data from Proctor et al. 2009; Forestell & Gebhardt 2010). It is an isolated E6 galaxy, with a velocity dispersion that generally shows a rapid decrease with radius (Romanowsky et al. 2003) and kinematic and photometric signatures of an edge-on stellar disk (Proctor et al. 2009).

NGC 1407 is a large, round, massive elliptical with a large velocity dispersion (Goudfrooij et al. 1994). Following Pota et al. (2013), we choose the red GCs out of 356 confirmed GCs and bin them in equal-number bins of about 20 objects. The velocity dispersion shows two positive deviations - one in the interval of 0.6  $R_{\text{eff}}$  and 2.5  $R_{\text{eff}}$ , the other one from 2.5  $R_{\text{eff}}$  to 4.8  $R_{\text{eff}}$  ( $R_{\text{eff}} = 9.36$  kpc, GCs data from Pota et al. 2013, stellar data from Proctor et al. 2009; Spolaor et al. 2008).

The GCs data of NGC 3115 were first presented by Arnold et al. (2011). This S0-galaxy contains a chemically enriched and kinematically distinct stellar disk

(Norris et al. 2006). The  $\sigma$ -bump can be seen in the range of 0.7 to 2.2  $R_{\text{eff}}$  ( $R_{\text{eff}}=3.87$  kpc). For NGC 4278 (GCs data from Pota et al. 2013, stellar data from van der Marel & Franx 1993) we observe a  $\sigma$ -bump in a large range: from 1.5 to 3.8  $R_{\text{eff}}$  ( $R_{\text{eff}} = 2.58$  kpc). This galaxy has a large HI disk and a dusty patch (Goudfrooij et al. 1994).

Additionally, we found a  $\sigma$ -bump feature in the galaxy NGC 4697. For this galaxy we found the most extended data set, with 218 PNe from Méndez et al. (2009) and 531 PNe from Méndez et al. (2001, 2008). The kinematic information covers the central area as well as the outer regions of the galaxy, showing a  $\sigma$ -bump behavior between 0.9 and 2.7  $R_{\text{eff}}$  ( $R_{\text{eff}} = 3.36$  kpc, stellar data from Binney et al. 1990). NGC 4697 is an E4-5 galaxy with a stellar disk along the major axis (Carter 1987; Goudfrooij et al. 1994) and at least two PNe subpopulations (Sambhus et al. 2006).

We thus conclude that the  $\sigma$ -bump is a feature that can be observed with tracers in the outer parts of ETGs in the stellar component, however a statistically significant amount of tracers is needed.

## 5. SUMMARY AND DISCUSSION

We have identified a new feature in the kinematics of ETGs, which can be seen in all spheroidals resulting from our sample of ten simulated isolated major mergers. The azimuthal component of the velocity dispersion contributes the most to the  $\sigma$ -bump, whereas shells are dominated by the radial dispersion component. This  $\sigma$ -bump can already be seen shortly after the merging event and remains stable with time, while other features such as shells vanish after a few Gyrs. We found the  $\sigma$ -bump to be a purely stellar feature which is not mirrored by the velocity dispersion of the dark matter component. The

$\sigma$ -bump is most prominent in 1:1 mergers and therefore might be a signature for major mergers.

Observations of some ETGs such as NGC 821, NGC 1407, NGC 3115, NGC 4278 and NGC 4697 show a positive deviation of the velocity dispersion in the same  $R_{\text{eff}}$ -range as our galaxies. In three out of these five galaxies, a stellar disc is observed, while a fourth galaxy has a HI disk. All galaxies from Pota et al. (2013) that show a  $\sigma$ -bump are fast rotators as well as NGC 4697 (Emsellem et al. 2011). In the sample of Pota et al. (2013), two of the three galaxies that do not show  $\sigma$ -bump are also fast rotators, one is a slow rotator.

The fact that the  $\sigma$ -bump is also present in galaxies which have been simulated without gas or bulge components suggests that it is a remnant of the kinematics of the disk stars of the progenitor galaxy. The region of the  $\sigma$ -bump is interesting, as it corresponds to the size of the disk of the progenitor galaxy. Between 7 kpc and 14 kpc (23 kpc for 31 OBH 09 320), the dark matter begins to dominate over the stellar component, which might also influence the dynamics of the stellar component. The reasons for the presence or absence of the  $\sigma$ -bump thus remain to be investigated.

In a future study (Schauer et al., in prep) we will in-

vestigate a larger sample of simulated galaxies, including spheroidals from minor mergers and cosmological simulations, in order to survey if the  $\sigma$ -bump is present only in major mergers and how it relates to the disk of the progenitor galaxies. It is interesting that we see a  $\sigma$ -bump also in the Sbc dry merger with 0% gas by Dekel et al. (2005), but in none of their other mergers, and at least in one of the galaxies with mass ratio of 1:1 from Jesseit et al. (2007).

The velocity dispersion is a quantity for which the accuracy strongly depends on the number of observed tracer objects. To understand which signatures about the formation history and evolution of ETGs are retained by their outer halos, more detailed observations of the outskirts of ETGs are required, especially larger observational tracer samples.

We thank the referee for many helpful comments. R.-S.R. acknowledges a grant from the International Max-Planck Research School of Astrophysics (IMPRS). A.T.P.S., R.-S.R. and A.B. acknowledge financial support from the cluster of excellence ‘‘Origin and Structure of the Universe’’. P.H.J. acknowledges the support of the Research Funds of the University of Helsinki.

#### REFERENCES

- Arnold, J. A., Romanowsky, A. J., Brodie, J. P., Chomiuk, L., Spitler, L. R., Strader, J., Benson, A. J., & Forbes, D. A. 2011, *ApJ*, 736, L26
- Arnold, J. A., Romanowsky, A. J., Brodie, J. P., Forbes, D. A., Strader, J., Spitler, L. R., Foster, C., Kartha, S. S., Pastorello, N., Pota, V., Usher, C., & Woodley, K. A. 2013, *ArXiv e-prints*
- Binney, J. & Tremaine, S. 2008, *Galactic Dynamics* (Princeton University Press), 2nd edition
- Binney, J. J., Davies, R. L., & Illingworth, G. D. 1990, *ApJ*, 361, 78
- Carter, D. 1987, *ApJ*, 312, 514
- Coccatto, L., Gerhard, O., Arnaboldi, M., Das, P., Douglas, N. G., Kuijken, K., Merrifield, M. R., Napolitano, N. R., Noordermeer, E., Romanowsky, A. J., Capaccioli, M., Cortesi, A., de Lorenzi, F., & Freeman, K. C. 2009, *MNRAS*, 394, 1249
- Cooper, A. P., Martínez-Delgado, D., Helly, J., Frenk, C., Cole, S., Crawford, K., Zibetti, S., Carballo-Bello, J. A., & GaBany, R. J. 2011, *ApJ*, 743, L21
- Cortesi, A., Merrifield, M. R., Coccatto, L., Arnaboldi, M., Gerhard, O., Bamford, S., Napolitano, N. R., Romanowsky, A. J., Douglas, N. G., Kuijken, K., Capaccioli, M., Freeman, K. C., Saha, K., & Chies-Santos, A. L. 2013, *MNRAS*, 432, 1010
- Dekel, A., Stoehr, F., Mamon, G. A., Cox, T. J., Novak, G. S., & Primack, J. R. 2005, *Nature*, 437, 707
- Douglas, N. G., Napolitano, N. R., Romanowsky, A. J., Coccatto, L., Kuijken, K., Merrifield, M. R., Arnaboldi, M., Gerhard, O., Freeman, K. C., Merrett, H. R., Noordermeer, E., & Capaccioli, M. 2007, *ApJ*, 664, 257
- Emsellem, E., Cappellari, M., Krajnović, D., Alatalo, K., Blitz, L., Bois, M., Bournaud, F., Bureau, M., Davies, R. L., Davis, T. A., de Zeeuw, P. T., Khochfar, S., Kuntschner, H., Lablanche, P.-Y., McDermid, R. M., Morganti, R., Naab, T., Oosterloo, T., Sarzi, M., Scott, N., Serra, P., van de Ven, G., Weijmans, A.-M., & Young, L. M. 2011, *MNRAS*, 414, 888
- Forestell, A. D. & Gebhardt, K. 2010, *ApJ*, 716, 370
- Foster, C., Arnold, J. A., Forbes, D. A., Pastorello, N., Romanowsky, A. J., Spitler, L. R., Strader, J., & Brodie, J. P. 2013, *ArXiv e-prints*
- Foster, C., Spitler, L. R., Romanowsky, A. J., Forbes, D. A., Pota, V., Bekki, K., Strader, J., Proctor, R. N., Arnold, J. A., & Brodie, J. P. 2011, *MNRAS*, 415, 3393
- Goudfrooij, P., Hansen, L., Jorgensen, H. E., Norgaard-Nielsen, H. U., de Jong, T., & van den Hoek, L. B. 1994, *A&AS*, 104, 179
- Hernquist, L. & Quinn, P. J. 1988, *ApJ*, 331, 682
- Hui, X., Ford, H. C., Freeman, K. C., & Dopita, M. A. 1995, *ApJ*, 449, 592
- Jesseit, R., Naab, T., Peletier, R. F., & Burkert, A. 2007, *MNRAS*, 376, 997
- Johansson, P. H., Burkert, A., & Naab, T. 2009a, *ApJ*, 707, L184
- Johansson, P. H. & Efstathiou, G. 2006, *MNRAS*, 371, 1519
- Johansson, P. H., Naab, T., & Burkert, A. 2009b, *ApJ*, 690, 802
- Khochfar, S. & Burkert, A. 2006, *A&A*, 445, 403
- Malin, D. F. 1977, *AAS Photo Bulletin*, 16, #...10
- McKee, C. F. & Ostriker, J. P. 1977, *ApJ*, 218, 148
- Méndez, R. H., Riffeser, A., Kudritzki, R.-P., Matthias, M., Freeman, K. C., Arnaboldi, M., Capaccioli, M., & Gerhard, O. E. 2001, *ApJ*, 563, 135
- Méndez, R. H., Teodorescu, A. M., & Kudritzki, R.-P. 2008, *ApJS*, 175, 522
- Méndez, R. H., Teodorescu, A. M., Kudritzki, R.-P., & Burkert, A. 2009, *ApJ*, 691, 228
- Naab, T. & Burkert, A. 2003, *ApJ*, 597, 893
- Naab, T., Khochfar, S., & Burkert, A. 2006, *ApJ*, 636, L81
- Napolitano, N. R., Romanowsky, A. J., Coccatto, L., Capaccioli, M., Douglas, N. G., Noordermeer, E., Gerhard, O., Arnaboldi, M., de Lorenzi, F., Kuijken, K., Merrifield, M. R., O’Sullivan, E., Cortesi, A., Das, P., & Freeman, K. C. 2009, *MNRAS*, 393, 329
- Navarro, J. F., Frenk, C. S., & White, S. D. M. 1997, *ApJ*, 490, 493
- Noordermeer, E., Merrifield, M. R., Coccatto, L., Arnaboldi, M., Capaccioli, M., Douglas, N. G., Freeman, K. C., Gerhard, O., Kuijken, K., de Lorenzi, F., Napolitano, N. R., & Romanowsky, A. J. 2008, *MNRAS*, 384, 943
- Norris, M. A., Sharples, R. M., & Kuntschner, H. 2006, *MNRAS*, 367, 815
- Peng, E. W., Ford, H. C., & Freeman, K. C. 2004, *ApJ*, 602, 685
- Pota, V., Forbes, D. A., Romanowsky, A. J., Brodie, J. P., Spitler, L. R., Strader, J., Foster, C., Arnold, J. A., Benson, A., Blom, C., Hargis, J. R., Rhode, K. L., & Usher, C. 2013, *MNRAS*, 428, 389
- Proctor, R. N., Forbes, D. A., Romanowsky, A. J., Brodie, J. P., Strader, J., Spolaor, M., Mendel, J. T., & Spitler, L. 2009, *MNRAS*, 398, 91

- Remus, R.-S., Burkert, A., Dolag, K., Johansson, P. H., Naab, T., Oser, L., & Thomas, J. 2013, *ApJ*, 766, 71
- Romanowsky, A. J., Douglas, N. G., Arnaboldi, M., Kuijken, K., Merrifield, M. R., Napolitano, N. R., Capaccioli, M., & Freeman, K. C. 2003, *Science*, 301, 1696
- Sambhus, N., Gerhard, O., & Méndez, R. H. 2006, *AJ*, 131, 837
- Schuberth, Y., Richtler, T., Hilker, M., Dirsch, B., Bassino, L. P., Romanowsky, A. J., & Infante, L. 2010, *A&A*, 513, A52
- Schweizer, F. 1986, *Science*, 231, 227
- Spolaor, M., Forbes, D. A., Hau, G. K. T., Proctor, R. N., & Brough, S. 2008, *MNRAS*, 385, 667
- Springel, V. 2005, *MNRAS*, 364, 1105
- Springel, V., Di Matteo, T., & Hernquist, L. 2005, *MNRAS*, 361, 776
- Springel, V. & Hernquist, L. 2003, *MNRAS*, 339, 289
- Strader, J., Romanowsky, A. J., Brodie, J. P., Spitler, L. R., Beasley, M. A., Arnold, J. A., Tamura, N., Sharples, R. M., & Arimoto, N. 2011, *ApJS*, 197, 33
- Toomre, A. 1978, in *IAU Symposium*, Vol. 79, Large Scale Structures in the Universe, ed. M. S. Longair & J. Einasto, 109–116
- van der Marel, R. P. & Franx, M. 1993, *ApJ*, 407, 525